GROUND TRUTH, MAGNITUDE CALIBRATION, AND REGIONAL PHASE PROPAGATION AND DETECTION IN THE MIDDLE EAST AND THE HORN OF AFRICA

Andrew A. Nyblade[1], Aubreya Adams[1], Richard A. Brazier[1], Yongcheol Park[1], and Arthur J. Rodgers[2]

Penn State University[1] and Lawrence Livermore National Laboratory[2]

ABSTRACT

In this project, we have exploited unique and open-source seismic datasets to improve seismic monitoring across the Middle East (including the Iranian Plateau, Zagros Mountains, Arabian Peninsula, Turkish Plateau, Gulf of Aqaba, Dead Sea Rift) and the Horn of Africa (including the northern part of the East African Rift, Afar Depression, southern Red Sea, and Gulf of Aden). The data sets have been used to perform two related tasks. (1) We have determined moment tensors, moment magnitudes, and source depths for regional events in the magnitude 4.0 to 6.0 range. (2) These events have been used to characterize high-frequency regional phase attenuation and detection thresholds, especially from events in Iran recorded at stations across the Arabian Peninsula.

In the first part of this project, seismograms from earthquakes in the Zagros Mountains recorded at regional distances have been inverted for moment tensors, and source depths for the earthquakes have been determined via matching regional waveforms using a grid search algorithm and forward modeling of teleseismic depth phases. Early studies of the distribution of seismicity in the Zagros region found evidence for earthquakes in the upper mantle. But subsequent relocations of teleseismic earthquakes suggest that source depths are generally much shallower, lying mainly within the upper crust. For all of the events that have been studied, source depths lie within the upper crust. And the events all have thrust mechanisms with E-W or NW-SE striking nodal planes. In the second part of this project, the source mechanisms for these events have been used to characterize high-frequency (0.5–16 Hz) regional phase attenuation and detection thresholds for broadband seismic stations in the Arabian Peninsula, including International Monitoring System (IMS) stations and stations belonging to the Saudi Arabian National Digital Seismic Network.

To improve event locations, source mechanisms, and attenuation estimates, new regional P- and S-wave velocity models of the upper mantle under the Arabian Peninsula have also been developed using data from teleseismic events recorded at stations within the Arabian Peninsula and the Horn of Africa. These models show slower-than-average velocities within the lithsopheric mantle under the entire Arabian Shield. However, at sublithospheric mantle depths, the low-velocity region appears to be localized beneath the western side of the Arabian Shield.

Report Documentation Page

1. REPORT DATE	2. REPORT TYPE	3. DATES COVERED
SEP 2008		**00-00-2008 to 00-00-2008**

4. TITLE AND SUBTITLE	5a. CONTRACT NUMBER
Ground Truth, Magnitude Calibration, and Regional Phase Propagation and Detection in the Middle East and the Horn of Africa	5b. GRANT NUMBER
	5c. PROGRAM ELEMENT NUMBER
6. AUTHOR(S)	5d. PROJECT NUMBER
	5e. TASK NUMBER
	5f. WORK UNIT NUMBER

7. PERFORMING ORGANIZATION NAME(S) AND ADDRESS(ES)	8. PERFORMING ORGANIZATION REPORT NUMBER
Lawrence Livermore National Laboratory,PO Box 808,Livermore,CA,94551-0808	

9. SPONSORING/MONITORING AGENCY NAME(S) AND ADDRESS(ES)	10. SPONSOR/MONITOR'S ACRONYM(S)
	11. SPONSOR/MONITOR'S REPORT NUMBER(S)

12. DISTRIBUTION/AVAILABILITY STATEMENT
Approved for public release; distribution unlimited

13. SUPPLEMENTARY NOTES
Proceedings of the 30th Monitoring Research Review: Ground-Based Nuclear Explosion? Monitoring?Technologies, 23-25 Sep 2008, Portsmouth, VA sponsored by the National Nuclear Security Administration (NNSA) and the Air Force Research Laboratory (AFRL)

14. ABSTRACT
see report

15. SUBJECT TERMS

16. SECURITY CLASSIFICATION OF:			17. LIMITATION OF ABSTRACT	18. NUMBER OF PAGES	19a. NAME OF RESPONSIBLE PERSON
a. REPORT **unclassified**	b. ABSTRACT **unclassified**	c. THIS PAGE **unclassified**	**Same as Report (SAR)**	**11**	

OBJECTIVE

The objective of this effort has been to determine ground truth source parameters (depth, moment, focal mechanism) for earthquakes in the Middle East. We have focused on events in the Zagros Mountains of Iran and used unique broadband waveforms from regional stations. Source moments are being used to calibrate coda wave moment magnitudes (Mayeda et al., 2003) and to model high-frequency regional body-wave amplitude spectra with the Magnitude-Distance Amplitude Correction (MDAC) methodology (Walter and Taylor, 2001). To help in this effort, we have also developed new velocity models of the upper mantle beneath the Arabian Peninsula.

RESEARCH ACCOMPLISHED

Introduction

In this project, we have exploited unique and open-source seismic data sets to improve seismic monitoring for the Middle East (including the Iranian Plateau, Zagros Mountains, Arabian Peninsula, Turkish Plateau, Gulf of Aqaba, Dead Sea Rift) and the Horn of Africa (including the northern part of the East African Rift, Afar Depression, southern Red Sea, and Gulf of Aden). Broadband waveform data sets have been used to perform three related tasks. (1) We have determined moment tensors, moment magnitudes, and source depths for regional events in the magnitude 3.0 to 6.0 range. (2) These events have been used to characterize high-frequency (0.5–16 Hz) regional phase attenuation and detection thresholds, especially from events in Iran recorded at stations across the Arabian Peninsula. (3) We have developed new velocity models of the upper mantle beneath the Arabian Peninsula. The results of this research enhance monitoring capabilities within the study region by improving our understanding of high frequency regional phase attenuation and how this attenuation affects detection thresholds, as well as the velocity structure of the uppermost mantle.

Towards meeting these objectives, seismograms from earthquakes in the Zagros Mountains recorded at regional distances have been inverted for moment tensors, which have then been used to create synthetic seismograms to determine the source depths of the earthquakes via waveform matching. The source depths have been confirmed by modeling teleseismic depth phases recorded on global seismographic network (GSN) and IMS stations. Early studies of the distribution of seismicity in the Zagros region found evidence for earthquakes in the upper mantle. But subsequent relocations of teleseismic earthquakes suggest that source depths are generally much shallower, lying mainly within the upper crust. All of the regional events studied nucleated within the upper crust, and most of the events have thrust mechanisms. The source mechanisms for these events have been used to characterize high-frequency (0.5–16 Hz) regional phase attenuation and detection thresholds for broadband seismic stations in the Arabian Peninsula, including IMS stations and stations belonging to the Saudi Arabian National Digital Seismic Network.

To improve event locations, source mechanisms and attenuation estimates, new regional P- and S-wave velocity models of the upper mantle under the Arabian Peninsula have also been developed using data from teleseismic events recorded at stations within the Arabian Peninsula and Horn of Africa. These models show slower-than-average velocities within the lithsopheric mantle under the entire Arabian Shield. However, at sublithospheric mantle depths, the low velocity region appears to be localized beneath the western side of the Arabian Shield.

Background

The Arabian Shield consists of a late Proterozoic crystalline basement overlain by Tertiary and Quaternary volcanic rocks in some places. The breakup of the Arabian Plate from Africa initiated at about 30–5 Ma, with the formation of the Red Sea–Gulf of Aden rift system (Coleman and McGuire, 1988). Volcanism was widespread between 30 and 12 Ma, and an uplift of the Arabian Shield occurred at about 13 Ma (Coleman and McGuire, 1988). The volcanism and uplift are thought to be related to the presence of a hot upper mantle (Camp and Roobol, 1992). The uplifted Arabian Shield contains two major features: one is the

Makkah-Madinah-Nafud (MMN) volcanic line in the south and the other is the Ha'il-Rutbah Arch in the north (Figure 1). The MMN volcanic line, extending north-south, has been the major site of volcanism in Saudi Arabia over the past 10 Ma, and the Ha'il-Rutbah Arch has been the site of several periods of uplift (Camp and Roobol, 1992).
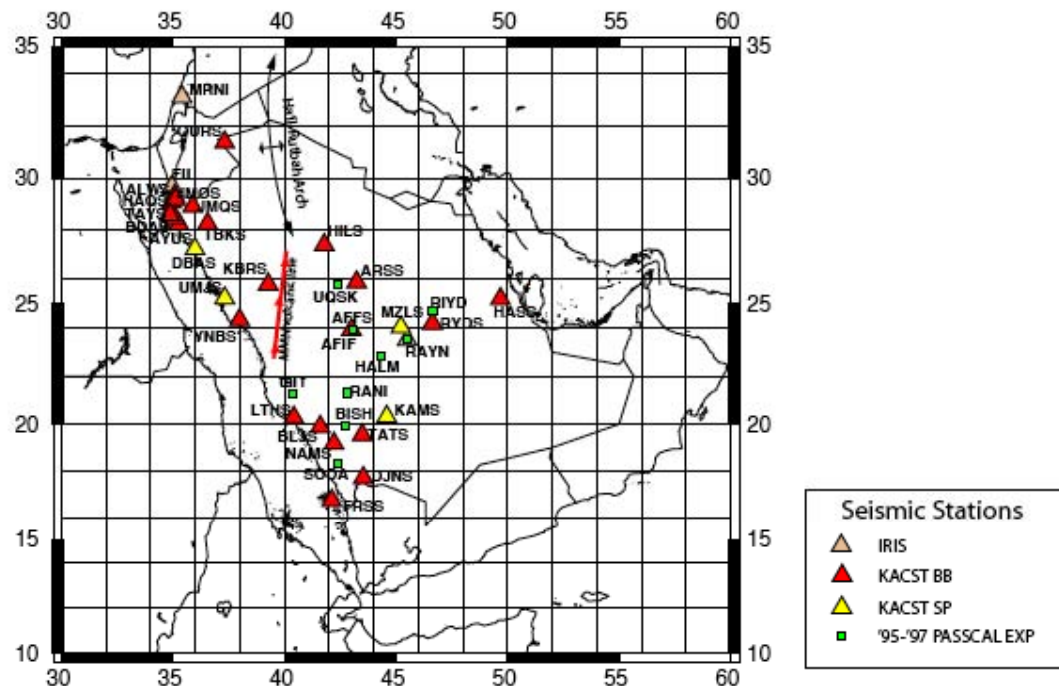
Figure 1. Map showing seismic stations in the Arabian Peninsula used in this study. KACST stations belong to the Saudi Arabia Digital National Seismic network.

The Zagros Mountain Belt, one of the world's most seismically active mountain ranges, marks the convergent boundary between the Arabian and Eurasian plates in southwestern Iran (Figure 2). The upper 11 km of the crust consists of folded sedimentary layers, while the lower 36 km of the crust are composed of faulted crystalline basement rock. The most prominent fault exposed at the surface is the Zagros Main Thrust, which marks the northern extent of seismicity associated with the Zagros Mountains and separates the Zagros Mountains from the Central Iranian Plateau. The Moho dips to the northeast from a depth of 40 km beneath the Persian Gulf to maximum depth of approximately 65–70 km beneath the Zagros Main Thrust (Hatzfeld et al., 2003). Early studies of the distribution of seismicity in the Zagros region found evidence for earthquakes in the upper mantle (Nowroozi, 1971; Bird et al., 1975). Subsequent recalculations of teleseismic earthquakes indicated that source depths were much shallower, lying within the upper crust (Maggi et al., 2000, 2002).

Zagros Earthquakes

Source depths and focal mechanisms for six well-studied events have been obtained (Tables 1 and 2). A grid-search method was used to determine the source parameters of each event. First, regional waveforms for each event were inverted for a moment tensor over a range of potential source depths. Synthetic seismograms were then computed using a reflectivity code for each source mechanism and compared to observed waveforms. In addition to the KACST and PASSCAL stations, data recorded at regional distances on open stations to the north and east were used, providing fairly good azimuth-ray coverage for each event. The quality of the visual fit between the synthetic and observed waveforms, along with the root-mean-square error, was used to determine the best-fitting focal mechanism and associated source depth. The velocity model used for the inversions is given in Table 3 and comes from Rodgers et al., (1999).

In addition, to help constrain focal depths, teleseismic depth phases from open stations in the 30 to 90 degree distance range were modeled using the focal mechanism obtained from the grid search at a particular depth. A local crustal model from Hatzfeld et al. (2003) was used for this modeling.

Figure 2. Colored topography map of the Middle East showing the location of the main plates and the Zagros Mountains.

The locations of the events are shown in Figure 3. Most of the events studied occurred within the central portion of the Zagros Mountains where there are the best constraints on crustal structure provided by receiver function and gravity studies. Figures 4a and 4b summarize graphically the results for two of the events, and serve to illustrate the quality of the waveform fits that we have obtained. Source depths for the events are within the upper crust.

Table 1. Source Parameters for Well-Studied Events in the Zagros Mountains (event letters are the same as in Figure 3)

Ev #	Date	Time	Lat (N), Long (E)	EHB	ISC		CMT		This Study	
				Depth (km)	Depth (km)	mb	Depth (km)	Mw	Depth (km)	Mw
A	11/13/98	13:01:10	27.79, 53.64	9	15.3	5.3	f33	5.4	4-7	5.5
B	10/31/99	15:09:40	29.41, 51.81	15	38	4.9	f33	5.2	4-5	5.4
C	3/1/00	20:06:29	28.39, 52.85	20	46.7	5.0	f15	5.0	7-10	5
D	2/17/02	13:03:53	28.09, 51.76	15	f15	5.5	f33	5.3	2-6	5.2
E	7/10/03	17:06:38	28.36, 54.17	11	19	5.8	f15	5.7	4-7	5.7
F	4/13/01	1:04:27	28.28, 54.87	20	28.7	4.9	26.1	5.1	8-11	4.9

International Seismic Centre (ISC) Catalog, Harvard Centroid Moment Tensor (CMT) Catalog, EHB (Engdahl et al., 2006); "f" indicates a fixed depth.

Table 2. Moment Tensor Elements for Specified Focal Depths

Ev #	Depth (km)	Mxx	Mxy	Mxz	Myy	Myz	Mzz	Mo
A	5	0.847e24	0.205e24	-0.152e25	0.634e23	0.753e24	-0.911e24	1.93E24
B	4	0.203e24	0.110e24	-0.107e25	0.236e24	0.705e24	-0.439e24	1.34E24
C	8	0.181e24	-0.397e23	-0.202e23	-0.167e23	0.278e24	-0.164e24	3.87E23
D	4	0.380e24	0.199e24	-0.393e24	0.550e23	0.561e24	-0.435e24	8.23E23
E	5	0.271e25	-0.212e24	0.225e25	-0.607e24	-0.328e25	-0.210e25	4.69E24
F	9	0.179e24	0.432e23	0.118e24	0.234e23	-0.300e23	-0.202e24	2.31E23

Table 3. Velocity Model Used for Moment Tensor Inversion

Depth (km)	P-wave Velocity (km/s)	S-wave Velocity (km/s)
1–4	4.00	2.31
4–20	6.22	3.59
20–38	6.44	3.72
38–42	7.30	4.21
42–74.5	8.04	4.48

Table 4. Velocity Model Used for Modeling Teleseismic Depth Phases

Depth (km)	P-wave Velocity (km/s)	S-wave Velocity (km/s)
1–11	4.700	2.714
11–19	5.850	3.378
19–46	6.500	3.753
46	8.000	4.620

A comparison of our results with previously reported magnitudes and source depths is provided in Table 1. The magnitude estimates obtained in this study are similar to those previously reported; however, the focal depths for a number of the events that we obtained are shallower than those reported in other catalogs.

The focal depth of earthquakes can affect the excitation of regional phases, particularly the guided Lg phase, which is composed of higher mode surfaces waves whose amplitudes are strongly depth dependent. The source parameters determined above can be used to infer how focal mechanism and depth might impact regional-phase S-wave generation and this might in turn impact P/S discriminants. Two nearby events (A and H) were recorded at station HILS on the northern Arabian Shield. Event A is the same event as in Table 1 and Figure 3. Event H was reported in Nyblade et al., (2006). These events had similar magnitudes (5.4 versus 5.7), and although both are thrust mechanisms, their strikes are slightly different. The high-frequency (0.5–5 Hz) response of these events is shown in Figure 5. Note that Lg is weaker with respect to the Pn for the deeper event (H), making the Pn/Lg ratio discriminant more explosion-like for this event. This suggests a possible depth-dependence of the Lg amplitude (and Pn/Lg ratio discriminant). Alternatively, the further event (H) may be located in a region of thicker crust, which leads to disruption of the crustal waveguide along the path to HILS. Both explanations would cause additional scatter in body-wave discriminants, compounding discrimination strategies.

Body-Wave Tomography

Upper mantle structure strongly impacts the propagation of regional Pn and Sn phases. We report velocity structure of the upper mantle reported from teleseismic P and S body-waves and from surface waves. To investigate upper-mantle structure under the Arabian Shield using body waves, we measured and inverted relative travel times from stations in Arabia. We augmented the KACST data with delay times measured from permanent stations in the region (RAYN, EIL and MRNI) and the 1995–1997 Saudi Arabian PASSCAL Experiment dataset. Figure 1 shows the locations of the seismic network used in this study. We computed travel time differences for two nearly colocated stations (AFFS and AFIF in Figure 1) between KACST and the PASSCAL networks in order to investigate possible biases between these data sets before combining all delay times from different seismic networks. We sorted events recorded on the common stations by back azimuth and distance and measured travel time residuals from arrival times subtracted from a theoretical travel time. The trends of the residuals with back-azimuth and distance are very similar and indicate no bias between the travel-time residuals for the common stations.
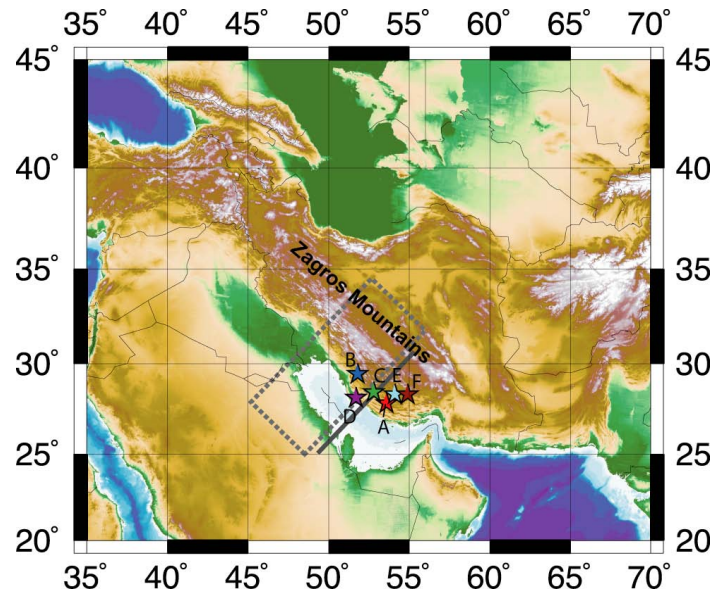
Figure 3. Map of Zagros Mountains and Persian Gulf showing the locations of earthquakes studied. Letters correspond to the events in Table 1. The grey box shows the area where crustal thickness has been constrained using gravity data, and the white line shows where crustal thickness has been imaged using receiver functions.
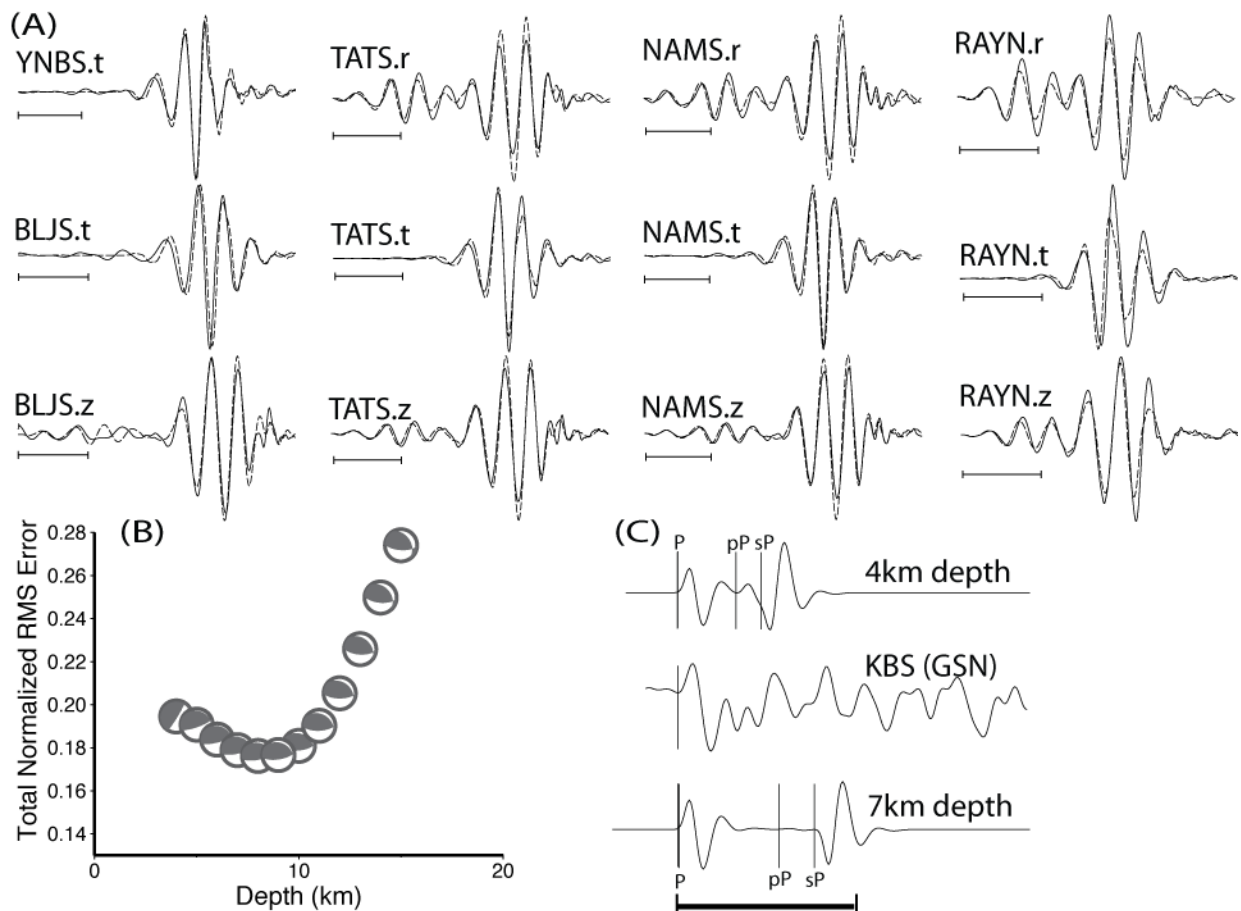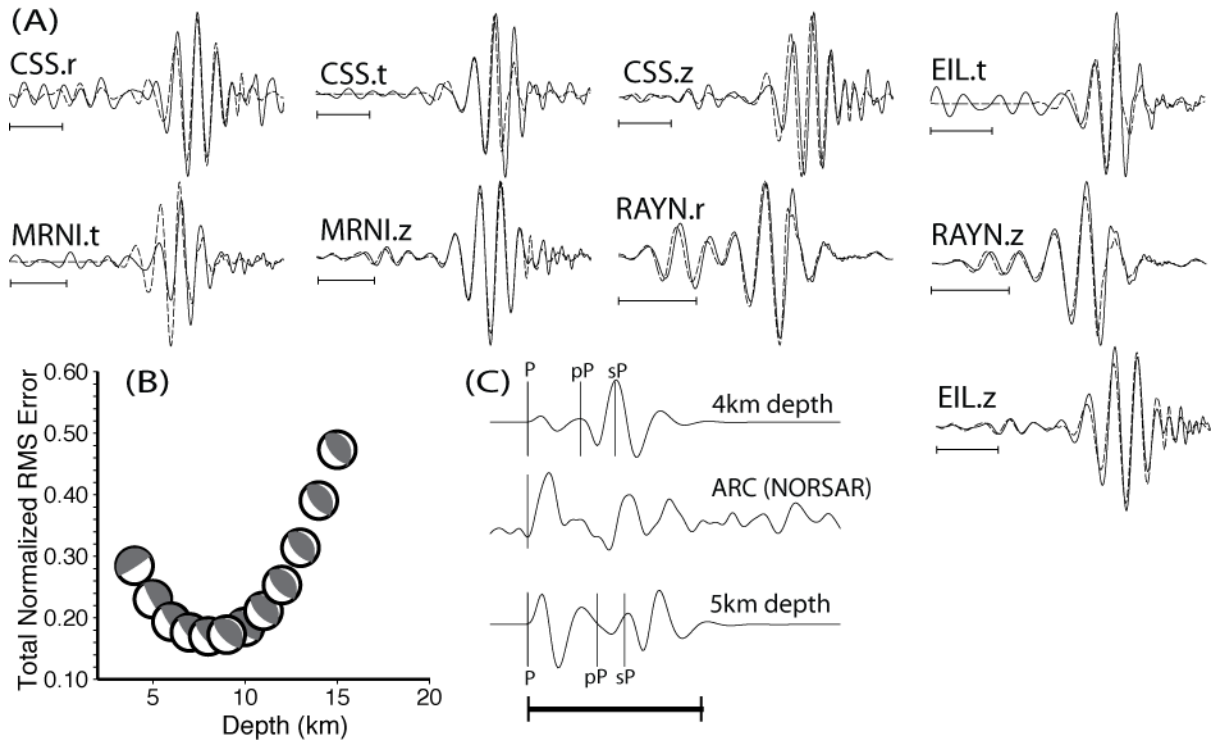

Figure 4a. Results for earthquake A, illustrating the method used for obtaining source parameters and the quality of the waveform fits. (A) Long-period regional displacement waveforms

(solid line) and synthetics (dashed line) for a number of stations. The scale bar shows 100 seconds. (B) Plot of focal depth vs. error. (C) Short-period teleseismic waveforms (data and synthetics), showing depth phases. The scale bar shows 5 seconds.

Figure 4b. Results for earthquake B illustrating the method used for obtaining source parameters and the quality of the waveform fits. (A) Long-period regional displacement waveforms (solid line) and synthetics (dashed line) for a number of stations. The scale bar shows 100 seconds. (B) Plot of focal depth vs. error. (C) Short-period teleseismic waveforms (data and synthetics) showing depth phases. The scale bar shows 5 seconds.
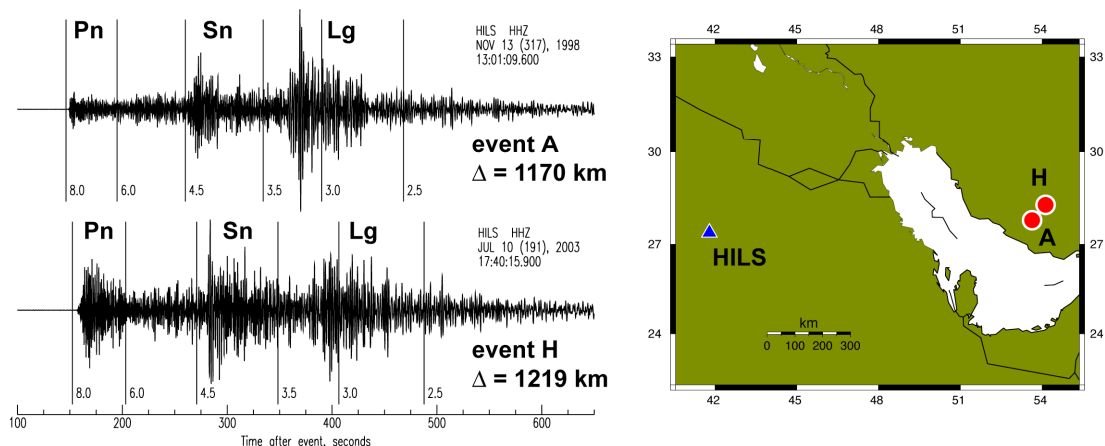

Figure 5. (Left) Vertical component waveforms (filtered 0.5–5 Hz) for events A (top) and H (bottom) at station HILS (Al Hail, Saudi Arabia). (Right) These events are closely located with event H slightly farther away.

For the datasets, we computed relative arrival-time residuals using a multichannel cross-correlation method (Crosson, 1990) and inverted for a three-dimensional velocity model using the method of VanDecar (1991). For the inversion, we parameterized travel-time slowness using a grid of knots composed of 34 knots in depth, 56 knots in latitude between 12.0° N, and 37.0° N and 56 knots in longitude between 29.5° E and 55.0° E. The horizontal knot spacing is one-third of a degree, and the vertical knot spacing is 25 km in the inner region of the seismic array (17.4° N–30.7° N, 35.5° E–48.5° E, and 0–200 km depth). We used the iasp91 model (Kennett and Engdahl, 1991) as the initial model for the inversion.

Results for the P-Wave Tomography

We used 401 earthquakes resulting in 3416 ray paths with P- and PKP-wave arrivals. The majority of the events are located in the western Pacific Rim between back azimuths of 15 and 150 degrees, but the events are distributed over a wide range of back azimuths. The waveforms were filtered with a zero-phase two-pole Butterworth filter between 0.5 to 2 Hz before the relative travel-time residuals were computed. The multichannel cross-correlation (MCCC) procedure was performed over a three-second window on the filtered data. A final model was selected by investigating the way in which changes in regularization levels (flattening and smoothing values) affect the reduction in travel-time residuals. To determine a preferred model, 2000 iterations of the conjugate gradient procedure are performed with several different pairs of flattening and smoothing values. For our preferred model, we have chosen a model with the values of 1600 for flattening and 3200 for smoothing. Figure 6 shows depth slices (a–d) and vertical cross-sections (e and f) through the P model. The first-order velocity variations seen in the S model are similar to the P model, and therefore we do not show the S-wave model here.
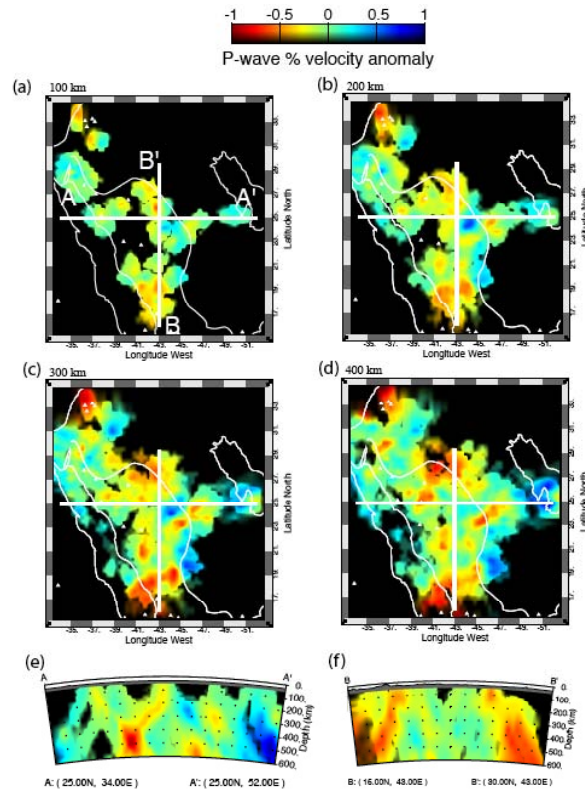
Figure 6. Results of P-wave tomography. (a–d) Depth slices through the model at depths of 100, 200, 300, and 400 km. (e–f) vertical slices through the model along E-W (e) and N-S (f) profiles denoted with white lines in a–d.

Surface-Wave Tomography

The shear-wave velocity structure of the shallow upper mantle beneath the Arabian Shield has been modeled by inverting Rayleigh-wave phase velocity measurements between 45 and 140 s together with previously published Rayleigh-wave group velocity measurements between 10 and 45 s (Park et al., 2008). For measuring phase velocities, we applied a modified array method to data from several regional networks that minimizes the distortion of ray paths caused by lateral heterogeneity. The new shear-wave velocity model shows a broad low-velocity region to depths of about 150 km in the mantle across the Shield and a narrower low-velocity region at depths greater than 150 km localized along the Red Sea coast and Makkah-Madinah-Nafud volcanic line. The results are shown in Figure 7.
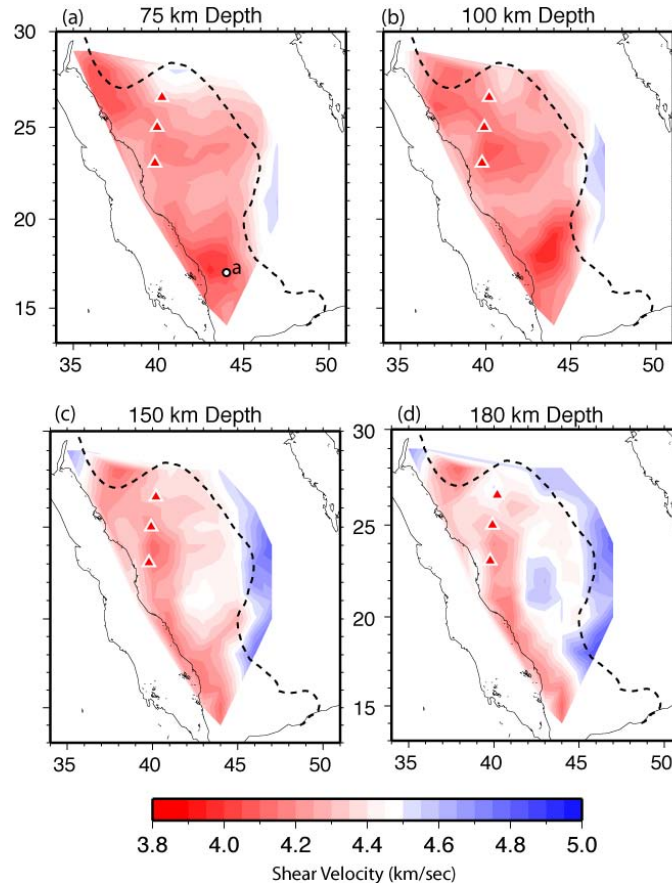
Figure 7. S-wave model of upper-mantle structure from inverting Rayleigh-wave phase velocities. (a–d) Horizontal slices through the model are shown for depths of 75, 100, 150, and 180 km. The red triangles show the location of the Makkah-Madinah-Nafud volcanic line. The dashed line shows the outline of the Shield.

CONCLUSIONS

We have obtained focal depths and mechanisms for several earthquakes in the Zagros Mountains. The source parameters for these events can be used to calibrate coda wave magnitudes and to model high-frequency regional phase amplitude spectra with the MDAC methodology. We have inverted teleseismic data (body and surface waves) to obtain new velocity models of the uppermost mantle under the Arabian Peninsula. These models show slower-than-average velocities within the lithsopheric mantle under the entire Arabian Shield. However, at sublithospheric mantle depths, the low-velocity region appears to be localized beneath the western side of the Arabian Shield.

REFERENCES

Bird, P., M. N. Toksoz, and N. H. Sleep (1975). Thermal and mechanical models of continent-continent convergence zones, *J. Geophys. Res*. 80: 4405–4416.

Camp, V. E. and M. J. Roobol (1992). Upwelling asthenosphere beneath western Arabia and its regional implications, *J. Geophys. Res.* 97: 15255–15271.

Coleman, R. G. and A. V. McGuire (1988). Magma systems related to the Red Sea opening, *Tectonophysics* 150: 77–100.

Crosson, R. S. (1990). Determination of teleseismic relative phase arrival times using multi-channel cross correlation and least-squares, *Bull. Seism. Soc. Am.* 80: 150–169.

Engdahl, E. R., J. A. Jackson, S. C. Myers, E. A. Bergman, and K. Priestley (2006). Relocation and assessment of seismicity in the Iran region, *Geophys. J. Int*. 222: 761–778.

Hatzfeld, D., M. Tatar, K. Priestley, and M. Ghafori-Ashtiany (2003). Seismological constraints on the crustal structure beneath the Zagros Mountain Belt (Iran), *Geophys. J. Int.* 155: 403–410.

Kennett, B. and E. R. Engdahl (1991). Travel times for global earthquake location and phase identification, *Geophys. J. Int.* 105: 429–465.

Maggi, A., J. Jackson, K. Priestley, and C. Baker (2000). A re-assessment of focal depth distributions in southern Iran, the Tien Sha and northern India: Do earthquakes really occur in the continental mantle? *Geophys. J. Int.* 143: 629–661.

Maggi, A., K. Priestley, and J. Jackson (2002). Focal depths of moderate to large earthquakes in Iran, *J. Seismol. Earthquake Eng*. 4: 1–10.

Mayeda, K., A. Hofstetter, J. O'Boyle, and W. Walter (2003). Stable and transportable regional magnitudes based on coda-derived moment-rate spectra, *Bull. Seism. Soc. Am*. 93: 224–239.

Nowroozi, A. A. (1971). Seismotectonics of the Persian Plateau Eastern Turkey, Caucasus, and Hindu-Kush regions, *Bull. Seism. Soc. Am*. 61: 317–342.

Nyblade, A., W. Walter, and R. Gok (2006). Developing and exploiting a unique seismic dataset from South African gold mines for source characterization and wave propagation, in *Proceedings of the 28th Seismic Research Review:Ground-Based Nuclear Explosion Monitoring Technologies,* LA-UR-0605471, Vol. 1, pp. 166–175.

Park, Y., A. A. Nyblade, A. J. Rodgers, and A. Al-Amri (2008). S wave velocity structure of the Arabian Shield upper mantle from Rayleigh wave tomography*, Geochem. Geophys. Geosyst.* 9: doi:10.1029/2007GC001895.

Rodgers, A. J., W. R. Walter, R. J. Mellors, A. M. S. Al-Amri, and U.-S. Zhang (1999). Lithospheric structure of the Arabian Shield and Platform from complete regional 256 waveform modelling and surface wave group velocities, *Geophys. J. Int*. 138: 871–878.

VanDecar, J. C. (1991). Upper mantle structure of the Cascadia subduction zone from non-linear teleseismic travel time inversion, Ph. D. thesis, Univ. of Washington, Seattle, WA.

Vernon, F. and J. Berger (1998). Broadband seismic characterization of the Arabian Shield, final scientific technical report, Department of Energy Contract No. F 19628-95-K-0015.

Walter, W. and S. Taylor (2001). A revised magnitude and distance amplitude correction (MDAC2) procedure for regional seismic discriminants, Lawrence Livermore National Laboratory technical report UCRL-ID-146882.